Driving missing data at the LHC: NNLO predictions for the ratio of γ+j and Z+j

John M. Campbell, R. Keith Ellis, and Ciaran Williams

Phys. Rev. D **96**, 014037 — Published 31 July 2017

DOI: 10.1103/PhysRevD.96.014037

IPPP/17/25, FERMILAB-PUB-17-085-T

Driving missing data at the LHC: NNLO predictions for the ratio of $\gamma + j$ and $Z + j$

John M. Campbell,[1,*] R. Keith Ellis,[2,†] and Ciaran Williams[3,‡]

[1] *Fermilab, P.O.Box 500, Batavia, IL 60510, USA*
[2] *Institute for Particle Physics Phenomenology, Department of Physics, University of Durham, Durham, DH1 3LE, UK*
[3] *Department of Physics, University at Buffalo The State University of New York, Buffalo 14260 USA*

In this paper we present a calculation of the $\gamma+j$ process at next-to-next-to-leading order (NNLO) in QCD and compare the resulting predictions to 8 TeV CMS data. We find good agreement with the shape of the photon p_T spectrum, particularly after the inclusion of additional electroweak corrections, but there is a tension between the overall normalization of the theoretical prediction and the measurement. We use our results to compute the ratio of $Z(\to \ell^+\ell^-) + j$ to $\gamma + j$ events as a function of the vector boson transverse momentum at NNLO, a quantity that is used to normalize $Z(\to \nu\overline{\nu}) + j$ backgrounds in searches for dark matter and supersymmetry. Our NNLO calculation significantly reduces the theoretical uncertainty on this ratio, thus boosting its power for future searches of new physics.

I. INTRODUCTION

One of the primary aims of the LHC's physics mission is to search for Beyond the Standard Model (BSM) physics. A key motivation for BSM physics arises from the cosmological observations of Dark Matter (DM). Thus far, multiple observations have inferred the existence of DM through its gravitational interactions with baryonic matter (see ref. [1] for a recent review); however to date no observation of non-gravitational interactions of DM has been conclusively established. The search for non-gravitational interactions of DM is hence an ongoing and exciting area of active research.

At the LHC the putative DM particle, or any similarly weakly-interacting BSM state, will not be directly observed by the LHC detectors. Instead the particle may be pair-produced in association with jets, that are observed in copious amounts at the LHC. If the DM particle couples to the SM through a heavy mediator then the typical transverse energy of the DM pair will be large, with the jets accounting for the corresponding recoil in the transverse plane. This would allow the presence of the DM to be inferred from an excess of events with large missing transverse energy (MET). As a result the MET+jets channel is one of the most exciting and rich channels in which to search for BSM effects (for a recent overview see ref. [2]).

Unfortunately, the Standard Model (SM) itself also provides a substantial source of events with large MET. The largest source of such events is through the production of a Z-boson in association with jets, with the subsequent decay $Z \to \nu\overline{\nu}$. Since the invisible decay forbids the reconstruction of the invariant mass of the parent Z-boson, this background cannot be easily suppressed by an explicit mass-window cut. This presents a significant challenge for MET+jet searches. Thankfully the visible decays of the Z provide a window through which to study this irreducible background [3, 4]. Decays of the Z boson to light charged leptons, $Z \to e^+e^-$ and $Z \to \mu^+\mu^-$, are clean experimental signatures with excellent resolution. By studying the impact of artificially not taking into account the visible leptons, the effect of the transition to MET-based observables can be easily quantified. However, a secondary issue arises when using the charged leptons as a tool to measure the neutrino background. Since the branching ratio for $Z \to \ell^+\ell^-$ is significantly smaller than for $Z \to \nu\overline{\nu}$ there are considerably less $Z \to \ell^+\ell^-$+jets events than MET+jets ones. At high vector boson transverse momentum (p_T^V), exactly the region of most interest, the low statistics of the $Z \to \ell^+\ell^-$ mode limits its utility for estimating the $Z \to \nu\overline{\nu}$ background.

In the region of high p_T^V one must therefore find an alternate strategy for calibrating the MET+jets background. One possibility is to make use of the sample of γ+jet events. The photon and Z boson are similar enough that a comparison of their production mechanisms is useful and, since one does not have to pay the price of a branching ratio for the photon, there is a factor of ~ 100 more events at high p_T. One can therefore measure the ratio of $\ell^+\ell^-$+jets and γ+jets events at low p_T and extrapolate into the high p_T^Z region. A good agreement between theory and data for this ratio is crucial; only once it has been demonstrated at lower values of p_T^V can the method be applied with confidence in the region of limited data at higher values of p_T^V.

Theoretical predictions for the $Z+j$ and $\gamma+j$ processes have been available at NLO for a long time [5, 6]. From these calculations the theoretical uncertainty associated with a truncation of the perturbative expansion at this order may be estimated from the sensitivity of the predictions to the choice of factorization, renormalization and (in the case of $\gamma+j$) fragmentation scales. These are typically in the range of 10–20%, which has been sufficient for

*Electronic address:johnmc@fnal.gov
†Electronic address:keith.ellis@durham.ac.uk
‡Electronic address:ciaranwi@buffalo.edu

testing the SM in these channels in the past. However, as the LHC accumulates more data of this nature [7–10], the experimental uncertainties are approaching the level of a few percent and will only decrease further. In order to achieve a similar level of theoretical precision it is necessary to include additional perturbative corrections. For the case of Z+jet production, NNLO QCD corrections have been extensively studied by now [11–14]. At this level of accuracy it is also necessary to include the effect of NLO electroweak corrections, which are also known for this process [15–18]. For γ+jet production, the closely-related direct photon process has recently been computed at NNLO in QCD [19] and the NLO EW corrections are known as well [20].

In this paper we will provide NNLO predictions for γ+jet production, thus bringing the theoretical prediction to the same level as for the Z+jet process. To do so we will make use of the direct photon calculation of Ref. [19], that has already been implemented in the Monte Carlo code MCFM, and explicitly demand the presence of a jet. With this calculation in hand we will be able to address the main aim of this paper, which is predicting the $\ell^+\ell^-$+jet/γ+jet ratio with an accounting of NNLO QCD and leading EW effects[1]. To do so we will also make use of the MCFM implementation of the NNLO corrections to Z+jet production [12].

II. CALCULATION

A. IR regularization

NNLO calculations require regularization of infrared singularities that are present in phase spaces with different numbers of final state partons. In our calculations we use the N-jettiness slicing approach that was outlined in refs. [22, 23], based on earlier similar applications to top-quark decay at NNLO [24]. This method follows a divide-and-conquer approach to regulating the singularities in the calculation. A cut on the N-jettiness variable τ_N [25] is introduced, where N is the number of jets in the Born phase space. For the case at hand $N = 1$. Therefore we introduce the following variable

$$\tau_1 = \sum_{k=1}^{M} \min_{i=a,b,1} \left\{ \frac{2q_i \cdot p_k}{Q_i} \right\} . \tag{1}$$

Where $\{p_k\}$ defines the momenta of the parton-level configuration, and $\{q_i\}$ represents the set of momenta that is obtained after application of a jet-clustering algorithm. The scale Q_i is a measure of the jet or beam hardness, which we take as $Q_i = 2E_i$. The labels a and b refer to the two beam partons. Note that if $\tau_1 = 0$ then the clustered momenta map directly onto the Born phase space (i.e. a one-jet configuration). Non-zero values of τ_1 therefore correspond to configurations with a greater number of partons than the Born phase space. We introduce a cut choice $\tau_1^{\rm cut}$ such that when $\tau_1 > \tau_1^{\rm cut}$ the components of the calculation contain at most single-unresolved infrared singularities. It therefore corresponds to a NLO calculation with an additional parton, albeit one which must be integrated with an extremely loose jet requirement. The double-unresolved singularities reside in the region $\tau_1 < \tau_1^{\rm cut}$, where the application of SCET [26–30] allows us to write the cross section as follows,

$$\sigma(\tau_1 < \tau_1^{\rm cut}) = \int \mathcal{H} \otimes \mathcal{B} \otimes \mathcal{B} \otimes \mathcal{S} \otimes \mathcal{J} + \mathcal{O}(\tau_1^{\rm cut}) . \tag{2}$$

That is, the cross section factorizes into a convolution of process-independent beam ($\mathcal{B}$) and jet ($\mathcal{J}$) functions, a soft function $\mathcal{S}$ (which depends on the number of colored scatterers) and a (finite) process-specific hard function $\mathcal{H}$. Expansions accurate to $\mathcal{O}(\alpha_s^2)$, that are relevant for our calculation, can be found in refs. [31, 32], [33, 34] and [35] for the beam, jet and soft functions respectively. The hard functions for the processes we consider in this paper are written in terms of the two-loop virtual matrix elements that have been calculated in ref. [36] and refs. [37, 38] for the γ+jet and Z+jet cases respectively. Their implementation has been discussed in ref. [12] for $Z + j$ production and in ref. [19] for direct photon production, which shares the same hard function as the photon+jet case we consider here. A key consideration within the N-jettiness slicing approach is the choice of $\tau_1^{\rm cut}$ used for the calculation. As indicated in Eq. (2), the below-cut factorization theorem receives power corrections that vanish in the limit $\tau_1^{\rm cut} \to 0$, but they can have a sizable impact on the cross section for non-zero values. Therefore it is crucial that $\tau_1^{\rm cut}$ be taken as small as possible, to minimize the impact of these corrections.[2] A general discussion of the process-specific parts of the direct photon and Z+jet calculations in MCFM was presented in refs [12, 19]. For brevity we will not reproduce that discussion here, but refer the interested reader to the original works for further details. Instead, in this paper we will focus on the validation of both calculations for the specific phase space selection criteria employed by the CMS analysis that we will follow.

B. Parameter choices

The usual MCFM EW parameter choice is the G_μ scheme, in which the values of M_W, M_Z and G_μ (the Fermi constant) are taken as inputs. In this scheme the

[1] Our work thus expands upon a recent comparison of combined NLO QCD+EW effects and CMS data that was performed as part of a Les Houches study [21].

[2] For recent work on reducing the dependence on power corrections, see refs. [39, 40].

electromagnetic coupling is then defined, at leading order, as

$$\alpha_{G_\mu} = \frac{G_\mu M_W^2 \sqrt{2}}{\pi}\left(1 - \frac{M_W^2}{M_Z^2}\right) \tag{3}$$

This is an appropriate choice for the description of $Z+j$ production, a process that is clearly sensitive to the electroweak scale. With the following choice of parameters,

$$\begin{aligned} M_Z &= 91.1876\,\text{GeV}\,, \qquad \Gamma_Z = 2.4952\,\text{GeV}\,, \\ M_W &= 80.385\,\text{GeV}\,, \qquad \sin^2\theta_w = 0.222897\,, \end{aligned} \tag{4}$$

the relation in Eq. (3) leads to a value of the electromagentic coupling,

$$\alpha|_{Z+j} = \alpha_{G_\mu} = 1/132.232\,. \tag{5}$$

For the calculation of $\gamma+j$ production, a process that involves a real photon in the final state, it is not clear that such a choice is the correct one.[3] For on-shell photons a natural alternative is provided by the $\alpha_{(0)}$ scheme in which the coupling is given by the fine-structure constant. Since we will later include the effects of NLO electroweak contributions for the $\gamma+j$ process that have been computed in this scheme [20] we choose,

$$\alpha|_{\gamma+j} = \alpha(0) = 1/137.036\,. \tag{6}$$

We will choose both renormalization (μ_R) and factorization (μ_F) scales equal to H_T, which is defined event-by-event to be the scalar sum of the transverse momenta of all partons, leptons and photons present. When studying the theoretical uncertainty associated with this choice of scale we consider a six-point variation corresponding to,

$$\mu_R = r H_T\,, \qquad \mu_F = f H_T\,, \tag{7}$$

with $r, f \in (\frac{1}{2}, 1, 2)$ and $rf \neq 1$. We use the NNLO CT14 set of parton distribution functions [43] for all predictions, where $\alpha_s(M_Z) = 0.118$ is taken from the PDF set. Studies of the associated PDF uncertainty are performed using the additional 56 eigenvector sets provided through LHAPDF6 [44] and are quoted at the 68% confidence level.

C. Event selection

Our phase space selection criteria are based on those used in a recent CMS analysis of 8 TeV data [45]. For the photon plus jets sample we require that the photon satisfies the following cuts

$$p_T^\gamma > 100\ \text{GeV}\,, \quad |\eta_\gamma| < 1.4\,. \tag{8}$$

[3] See for instance the discussion in Section 4.5.2 of Ref. [41].

Both experimentally and theoretically photons require isolation from hadronic activity. On the experimental side this reduces unwanted backgrounds from pion decays and photons that arise from fragmentation processes. Theoretically the calculation is simplified if smooth cone isolation [46] is employed. In that case one requires that the photon satisfies

$$\sum p_T^{\text{had}}(R) < \epsilon_\gamma p_T^\gamma \left(\frac{1-\cos R}{1-\cos R_0}\right)^n \quad \forall R < R_0\,. \tag{9}$$

This requirement constrains the sum of the hadronic energy inside a cone of radius R, for all separations R that are smaller than a chosen cone size, R_0. Cones are defined in terms of the R variable,

$$R = \sqrt{\Delta\eta^2 + \Delta\phi^2}\,, \tag{10}$$

where η and ϕ are the pseudorapidity and azimuthal angle of the particle, respectively. Note that arbitrarily soft radiation will always pass the condition, but collinear ($R \to 0$) radiation is forbidden. This removes the collinear splittings associated with fragmentation functions, at the cost of no longer reproducing the form of isolation applied in experimental analyses. In this paper we set $\epsilon_\gamma = 0.025$, $R_0 = 0.4$ and $n = 2$ in Eq. (9). This matches the parameters employed in a similar analysis by the BlackHat collaboration [3].[4] At NLO we can explicitly quantify the difference between following this procedure and performing a calculation that includes the effects of fragmentation. We shall see later that this difference is small, around a percent in the photon p_T spectrum.

In addition to the photon requirements described above, we require the presence of at least one jet in the event. Jets are defined using the anti-k_T [48] algorithm with $R = 0.5$ and satisfy,

$$p_T^j > 30\ \text{GeV}\,, \quad |\eta_j| < 2.4\,. \tag{11}$$

Additionally we require that photons and jets are separated by $R_{\gamma j} > 0.5$.

For the $Z+j$ sample we require that the charged leptons are in the following fiducial volume,

$$p_T^\ell > 20\ \text{GeV}\,, \quad |\eta_\ell| < 2.4\,. \tag{12}$$

We require that the lepton pair resides in an invariant mass window close to the Z mass, $71 < m_{\ell\ell} < 111$ GeV, and that the leptons are isolated from jets, $R_{\ell j} > 0.5$. We also require that $p_T^Z > 100$ GeV and $|y_Z| < 1.4$ to mimic the photon selection as closely as possible.

[4] We note that these parameters are slightly different to those used in previous MCFM studies of photonic processes at NNLO [19, 47]. We have compared with the alternative choice $\epsilon_\gamma = 0.1$ and found that the cross section only changes by around 1%.

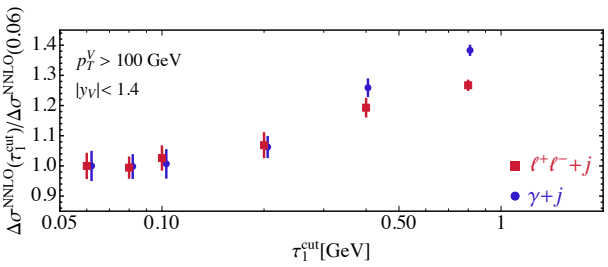

Figure 1: The dependence of the NNLO coefficient on the parameter $\tau_1^{\rm cut}$ for the processes considered in this paper. The cuts of the CMS analysis [45] have been applied. To aid visibility, the values of $\tau_1^{\rm cut}$ for the $\gamma + j$ calculation have been offset slightly.

D. $\tau_1^{\rm cut}$ dependence

Before providing NNLO predictions for γ+j (and Z+j) production we first validate our calculation for the phase space cuts described in the previous section. Since the N-jettiness slicing method is sensitive to power corrections it is crucial to validate the calculation for a new phase space selection. At NNLO the cross section can be written as

$$\sigma_{NNLO} = \sigma_{NLO} + \Delta\sigma_{NNLO}, \tag{13}$$

where σ_{NLO} is the NLO cross section and $\Delta\sigma_{NNLO}$ represents the correction that arises at NNLO. In MCFM, σ_{NLO} is calculated using a traditional Catani-Seymour dipole subtraction method [49] and only $\Delta\sigma_{NNLO}$ is computed using N-jettiness slicing. Therefore only $\Delta\sigma_{NNLO}$ has a dependence on $\tau_1^{\rm cut}$, a sensitivity that is indicated in Fig. 1. This figure shows the ratio $\Delta\sigma_{NNLO}(\tau_1^{\rm cut})/\Delta\sigma_{NNLO}(\tau_1^{\rm cut} = 0.06$ GeV), for both of the processes considered in this paper. Since the cuts have been chosen to emphasize the similarity between the two processes we see that, as expected, the dependence on $\tau_1^{\rm cut}$ is also comparable. Below $\tau_1^{\rm cut} = 0.1$ GeV the predictions are insensitive to the choice of $\tau_1^{\rm cut}$ within Monte Carlo uncertainties which, in this region, are around 5%.[5] We will see that $\Delta\sigma_{NNLO}/\sigma_{NNLO}$ is approximately 5–10% for both processes, so that the resulting uncertainty on σ_{NNLO} due to power corrections and Monte Carlo statistics is below 1%. This is perfectly acceptable for phenomenological purposes and, given the results in Fig. 1, we choose $\tau_1^{\rm cut} = 0.08$ GeV to compute the remainder of the results in this paper.

[5] We note that the MC uncertainties are all rescaled by the central value at $\tau_1^{\rm cut} = 0.06$ GeV such that there is no reduction in uncertainties due to the fact that the plotted quantity is a ratio.

E. Electroweak corrections

Since datasets at the LHC now permit the study of γ+jet and Z+jet events in which the photon or Z-boson carries a transverse momentum approaching 1 TeV, it is imperative to also account for the effect of electroweak corrections in theoretical predictions for these processes. Although these are generically expected to be rather small, at such high transverse momenta they give rise to Sudakov-enhanced corrections of the order of 10% or more. These primarily arise from the contribution of loop diagrams in which a virtual W- or Z-boson is exchanged, resulting in leading logarithms of the form $\log^2(M_V/p_T)$, whose effects on these processes have been known for some time [15, 16, 20]. More recently these effects have also been computed in the framework of SCET [50, 51]. We note that the effect of photon radiation from leptons is not captured in any of these calculations.

In this paper we shall make use of the results of Refs. [16, 20] in order to account for electroweak effects. The impact of the electroweak corrections can be captured by expressing their effect on the cross section (σ_{EW}) as a fraction of the leading order result,

$$\Delta_{\rm EW} = \frac{\sigma_{EW}}{\sigma_{LO}}\,. \tag{14}$$

We will treat the EW corrections as factorizing fully with respect to the QCD ones and simply multiply our NNLO QCD predictions by $1 + \Delta_{\rm EW}$. The calculation of σ_{EW} is performed using expressions that are valid in the high-energy limit and are NNLL accurate; these are specified in Section 3.5 of Ref. [16] and Section 3.3 of Ref. [20]. We have checked that this calculation agrees well with the results presented in Refs. [50, 51], up to numerical differences that are negligible for $\gamma + j$ production and are less than 1% for $Z + j$.

III. DIFFERENTIAL PREDICTIONS FOR $\gamma + j$

Before arriving at the primary interest of this paper, an analysis of the $Z + j/\gamma + j$ ratio at NNLO, we first consider the $\gamma + j$ process on its own. As discussed in the introduction, the $Z + j$ process has been extensively studied at NNLO, including detailed phenomenological analyses [11–14]. No such studies exist for the $\gamma + j$ process at this order and a careful analysis is a prerequisite to studying the ratio in detail. Therefore in this section we compare the predictions of MCFM for $\gamma + j$ production to CMS data collected at 8 TeV. The fundamental quantity of interest is the photon transverse momentum spectrum, which we present in Fig. 2. The correction from NLO to NNLO is around 10% and the NNLO prediction lies just at the very top of the scale variation band obtained at NLO. The NNLO/NLO K-factor is reasonably flat, with a slight increase at higher p_T. The scale

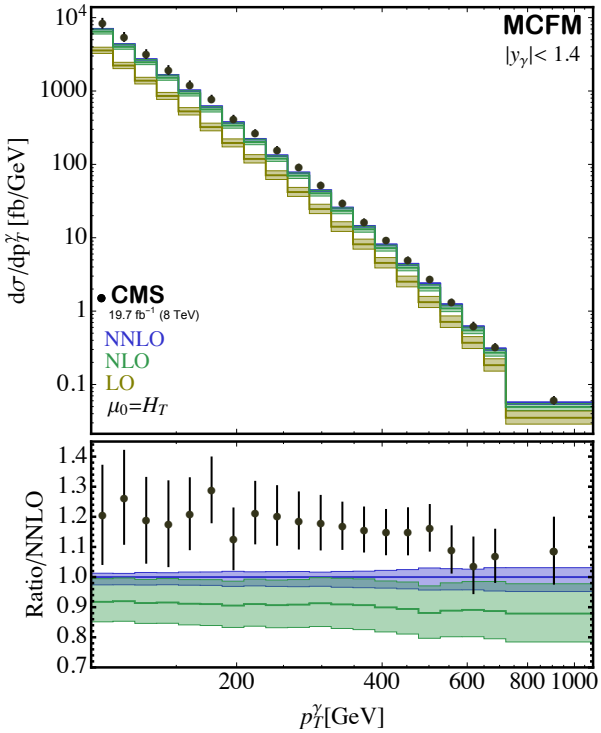

Figure 2: The photon p_T spectrum for $\gamma + j$ at the 8 TeV LHC, at various orders in perturbation theory, compared to CMS data from ref. [45]. The lower panel shows the ratio of the data and the NLO prediction to the NNLO one. The bands indicate the scale uncertainty on the NLO and NNLO predictions.

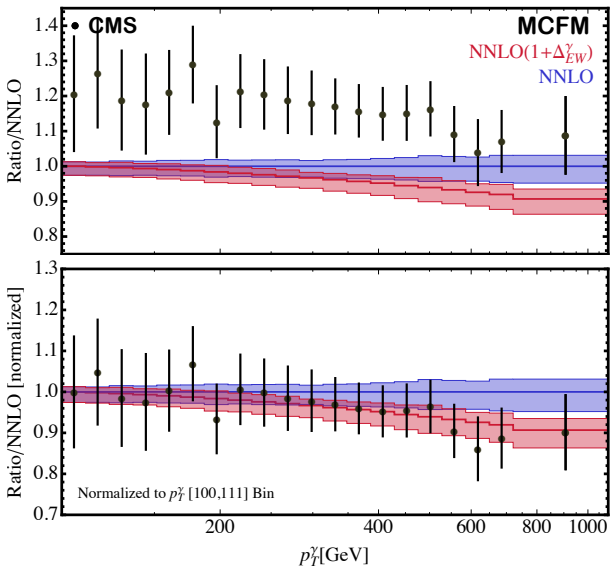

Figure 3: The ratio of the CMS data from ref. [45] to the NNLO prediction (with and without including EW effects) for the photon p_T spectrum. The lower panel normalizes this ratio to the value of the ratio in the [100, 111] bin.

variation at NNLO is significantly reduced compared to that obtained at NLO, with a typical variation of 2-3% compared to 8-10% at NLO. Although the NNLO prediction lies closer to the CMS data than the NLO one, both predictions are consistently lower than the experimental measurements.

We now include the effect of electroweak corrections as discussed above, by rescaling the complete NNLO result by the change observed in the LO prediction when including one-loop electroweak effects. We denote this combination by the shorthand NNLO(1+$\Delta_{\rm EW}$). Fig. 3 shows the ratio of data and NNLO(1+$\Delta_{\rm EW}$) to the pure NNLO prediction for the photon p_T spectrum. The upper panel shows the raw ratio, while the lower panel normalizes all predictions to their central value in the $p_T^\gamma \in [100, 111]$ GeV bin, allowing us to compare the shape of the predictions. We note that this procedure results in an overestimate of the errors on the CMS data, since a normalized distribution should not be sensitive to the overall luminosity. However, for the purposes of this comparison this overestimate can be tolerated. However, a full analysis of the shape of the distribution measured by the LHC collaborations and a comparison to its theory counterparts is clearly very desirable. The upper panel shows that, by including the EW corrections, the apparent agreement between theory and data gets worse. However, the lower panel shows that the shape of the data and theory predictions are actually in very good agreement.

We have so far only considered the theoretical uncertainty originating from the choice of scale and demonstrated that it is significantly reduced at NNLO, by a factor of two. However there are other origins of theoretical uncertainty, beyond scale variation, that affect our prediction. We will now consider two other sources of theoretical uncertainty: the choice of PDFs and the form of the photon isolation. These may primarily affect the normalization of the theoretical prediction, or may induce changes in the shape of the distributions. For PDF uncertainties we will consider the 68% confidence level uncertainties provided by LHAPDF6 [44] where, for efficiency, these uncertainties are computed from the NLO prediction (using NNLO CT14 PDFs). We have checked that the difference in PDF uncertainty obtained from LO and NLO calculations using this set is very small, so that we are confident that this provides a reliable estimate of the PDF uncertainty for our NNLO prediction. In order to quantify the effect of the difference between our isolation prescription and that of the experimental analysis, we repeat our NLO calculation using the parton-level version of the experimental isolation procedure:

$$E_T^{\rm had} < 5\,{\rm GeV} \quad \forall R < R_0\,. \tag{15}$$

Here, as in the smooth cone version, $R_0 = 0.4$ and our calculation employs the GdRG fragmentation functions [52]. Since the difference between the methods of isolating the photon could be affected differently at

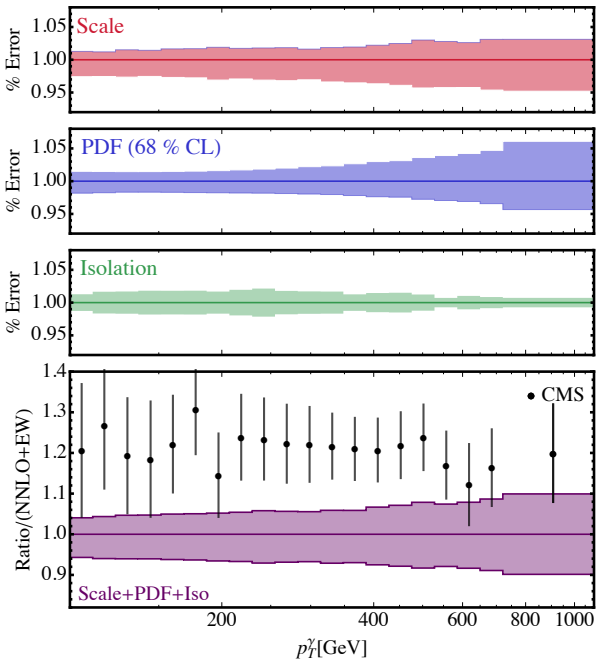

Figure 4: A summary of the theoretical uncertainties discussed in this paper for the photon transverse momentum spectrum. In order from the top, uncertainties from: scales, PDFs, isolation and in the total, as described in the main text. The total uncertainty is obtained by combining linearly those from the sources above.

NNLO we should provide a conservative estimate of this effect. We therefore estimate the isolation uncertainty by taking the difference between the two isolation procedures, multiplying by an additional factor of two, and allowing excursions from our central result by this amount on either side.

Our results for the uncertainty in the theoretical prediction for the photon p_T spectrum are presented in Figure 4. The uncertainties are normalized to the central value of the combined NNLO QCD + NLO EW prediction. We observe that at NNLO the scale variation and PDF uncertainty are roughly equal and correspond to a few percent uncertainty. The PDF uncertainty grows more rapidly as a function of photon transverse momentum and is largest in the highest bins ($\sim$ 5%). The uncertainty stemming from the isolation procedure is at the level of 2% for lower values of p_T^γ but is significantly smaller in the tail. This is in line with previous studies of the difference between smooth cone isolation and the forms used in experimental analyses [19, 53]. The total uncertainty from scales, PDFs and isolation, obtained by adding the individual uncertainties linearly, ranges from around 4% at low p_T^γ to 9% in the highest bins. Clearly the large PDF uncertainty can be reduced in the future [54, 55], by taking advantage of calculations such as this one in tandem with the even bigger $\gamma + j$ data sets being accumulated at the LHC.

The tension that remains between the data and our theoretical prediction, displayed in the lower panel of Figure 4, could have a number of sources. Although we have endeavored to be thorough, the accounting of theoretical uncertainty could yet be deficient. On the experimental side the normalization of the data could be changed by a host of factors, including a reduction in the overall luminosity, a change in the photon efficiency, or an issue with background subtraction.[6]

A further interesting observable to consider is the ratio of inclusive $\gamma+2j$ to $\gamma+j$ production as a function of the photon transverse momentum. Fixed-order calculations of this ratio can be broken down into contributions proportional to the relevant powers of the strong coupling as follows,

$$R_{2/1}(p_T^\gamma) = \frac{\alpha_s^2 \sum_{k=0}^{n_2} \alpha_s^k \, d\sigma^{(k)}_{\gamma+2j}/dp_T^\gamma}{\alpha_s \sum_{k=0}^{n_1} \alpha_s^k \, d\sigma^{(k)}_{\gamma+j}/dp_T^\gamma} \,. \qquad (16)$$

In this expression we have made clear that contributions to the denominator start with one power of α_s and those to the numerator with two. An inclusive calculation of $\gamma + j$ production, such as the one we are considering in this paper, naturally contains terms in the numerator up to $n_2 = n_1 - 1$. Our NNLO calculation corresponds to $n_1 = 2$ while the equivalent result from our NLO calculation is given by $n_1 = 1$. We call these predictions $R_{2/1}^{NNLO}$ and $R_{2/1}^{NLO}$ respectively and compare them to the CMS measurement of the same ratio in Fig. 5. $R_{2/1}^{\rm NLO}(p_T^\gamma)$ does a poor job of describing the data because it is a LO calculation for this observable and thus bears all the hallmarks of such a calculation. This is not only reflected by a general underestimation of the data, but also by the rather large scale dependence. The corrections to this ratio when moving to $R_{2/1}^{\rm NNLO}(p_T^\gamma)$ are large, around 30%. The agreement with data is significantly improved and the scale uncertainty is reduced by a factor of two.

However, from Eq. (16) it is clear that neither of the predictions presented so far corresponds to a strict expansion of the *ratio* to a given power of the strong coupling, due to the fact that the denominator contains an additional term of one order higher than the numerator. Instead we can define alternative predictions, corresponding to $n_2 = n_1$, with $R_{2/1}^{NLO\star}$ given by $n_1 = n_2 = 1$. Note that the alternative definition $R_{2/1}^{NLO\star}$ can be obtained by simply taking the ratio of two NLO calculations of $\gamma+2j$

[6] We note that the CMS paper [45] indicates a flat 2.6% luminosity uncertainty over the whole p_T^γ range, which is far below the level of disagreement indicated here.

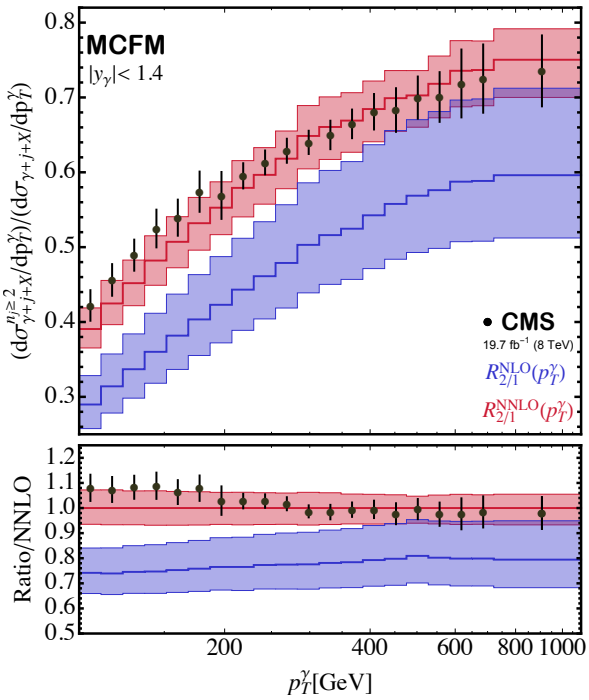

Figure 5: The quantities $R_{2/1}^{\rm NLO}(p_T^\gamma)$ and $R_{2/1}^{\rm NNLO}(p_T^\gamma)$ compared to CMS data from ref. [45]. The bands indicate the scale uncertainty on the theoretical predictions.

and $\gamma + j$ production. This is the procedure already followed by CMS [45] using the results of Ref. [3]. Since the NNLO corrections to $\gamma + 2j$ production are unknown, and likely to remain so for some time, it is useful to estimate the potential impact that they could have on the theoretical prediction for $R_{2/1}$. We do so by postulating NNLO corrections given by,

$$d\sigma_{\gamma+2j}^{(2,\text{approx})}/dp_T^\gamma = \pm\frac{\left[d\sigma_{\gamma+2j}^{(1)}/dp_T^\gamma\right]^2}{d\sigma_{\gamma+2j}^{(0)}/dp_T^\gamma}\,, \qquad (17)$$

where, as indicated, the corrections can be of either sign. In this way the NNLO corrections are of the same size relative to NLO as the NLO ones are to LO. A comparison of the results for $R_{2/1}^{NLO\star}$ and the two bounding estimates of $R_{2/1}^{NNLO\star}$, with both our calculation of $R_{2/1}^{NNLO}$ and the CMS data, is shown in Fig. 6. We see that, as observed already in ref. [45], the prediction $R_{2/1}^{NLO\star}$ is in good agreement with the data for $p_T^\gamma < 200$ GeV but overshoots it by around 15% at high p_T^γ. The range of the estimate $R_{2/1}^{NNLO\star}$ brackets both the theory predictions $R_{2/1}^{NLO\star}$ and $R_{2/1}^{NNLO}$, as well as the data, and is of a similar size as the scale uncertainty on $R_{2/1}^{NNLO}$ shown in Fig. 5. In addition, the data suggests that NNLO corrections to $\gamma+2j$ production might be expected to be small at high p_T^γ. In summary, $R_{2/1}^{NNLO}$ provides a fairly good description of the data and we believe that the associated scale uncertainty provides a plausible envelope for

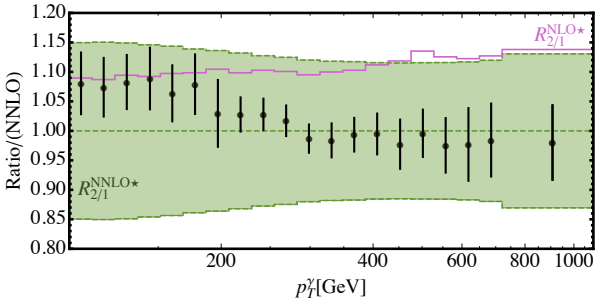

Figure 6: The quantity $R_{2/1}^{\rm NLO*}(p_T^\gamma)$, a range of estimates for $R_{2/1}^{\rm NNLO*}(p_T^\gamma)$ computed as discussed in the text, and the CMS measurements [45]. All quantities are normalized to the theoretical prediction $R_{2/1}^{\rm NNLO}(p_T^\gamma)$.

the results of a complete NNLO calculation of this ratio ($R_{2/1}^{NNLO*}$).

IV. THE Z/γ RATIO AT NNLO

We are now able to address the principal aim of this paper, which is improving the theoretical prediction for the ratio of $Z + j$ and $\gamma + j$ production. We consider the case where the Z boson decays to leptons and the two processes are studied in a similar kinematic regime by application of the cuts described in section II C. Specifically, we consider predictions for the quantity,

$$R_{Z/\gamma}^{\mathcal{O}}(p_T) = \frac{d\sigma_{\ell^-\ell^++j+X}^{\mathcal{O}}/dp_T}{d\sigma_{\gamma+j+X}^{\mathcal{O}}/dp_T}\,, \qquad (18)$$

where p_T represents the transverse momentum of the Z-boson or photon. A simple expectation for the behaviour of this ratio can be obtained by considering only the effect of the different Z and photon couplings, together with the effect of the PDFs, in the LO cross-section. This neglects the effect of the Z-boson mass, which should be irrelevant at large p_T^Z, as well as the impact of higher-order corrections. The ratio is then estimated to be [4],

$$R_{Z/\gamma} = \left(R_u + \frac{R_d - R_u}{1 + \frac{Q_u^2}{Q_d^2}\frac{\langle u\rangle}{\langle d\rangle}}\right)\left[\text{Br}(Z\to\ell^-\ell^+)\times\mathcal{A}\right]\,, \qquad (19)$$

where R_q is the relevant ratio of quark-boson couplings squared,

$$R_q = \frac{v_q^2 + a_q^2}{4\sin^2\theta_w\cos^2\theta_w Q_q^2}\,, \qquad (20)$$

and $\langle u\rangle$ ($\langle d\rangle$) is the typical up (down) quark PDF at the value of x probed by a given p_T^V, i.e. $\langle x\rangle = 2p_T^V/\sqrt{s}$. The branching ratio and acceptance factor ($\mathcal{A}$) account for the Z-boson decay and cuts on the leptons. At high

transverse momentum, $p_T^V \gg M_Z$, $x \to 1$ and $\langle u \rangle / \langle d \rangle \to \infty$, so that $R_{Z/\gamma}$ should slowly approach an asymptotic value from above [3, 4]. This argument thus predicts a plateau at high transverse momentum, which we will observe shortly in our full prediction. We stress that in our calculation this ratio is not computed for on-shell Z bosons but includes the decay into leptons, off-shell effects and the (small) contribution from virtual photon exchange. Nevertheless, we will refer to this quantity as $R_{Z/\gamma}$, or the Z/γ ratio, as a matter of convenience.

When computing this ratio a subtlety arises when trying to provide an uncertainty estimate based on scale variation. If the variation is correlated, i.e. one computes the scale uncertainty using the same scale in both the numerator and denominator of Eq. (18), then one obtains essentially no uncertainty on $R_{Z/\gamma}(p_T)$, even at NLO. We therefore discard this choice as a useful measure of the theoretical uncertainty. The alternative that we use instead is to consider variations of the scale in the numerator and denominator separately,

$$\frac{d\sigma^{\mathcal{O},\{r,f\}}_{\ell^-\ell^+ + j + X}/dp_T}{d\sigma^{\mathcal{O},r=f=1}_{\gamma + j + X}/dp_T} \quad \text{and} \quad \frac{d\sigma^{\mathcal{O},r=f=1}_{\ell^-\ell^+ + j + X}/dp_T}{d\sigma^{\mathcal{O},\{r,f\}}_{\gamma + j + X}/dp_T}\,, \tag{21}$$

where $\{r, f\}$ represents the six-point scale variation indicated in Eq. (7). The uncertainty is then defined by the extremal values of either of these two ratios. In practice, since the scale-dependence of the two processes is so similar, this procedure is almost identical to defining the uncertainty in terms of the variation of either quantity in Eq. (21) alone. In contrast to the correlated variation, this approach results in scale uncertainties that, order-by-order, overlap both the data and the central result of the next-higher order. Moreover, with this procedure, at NNLO the resulting uncertainty band is of a size typical of a NNLO prediction and still smaller than the experimental uncertainties.

Our results for the ratio for the pure QCD NLO and NNLO calculation are shown in Fig. 7. The most significant effect of the NNLO calculation is to decrease the ratio, particularly at lower values of p_T. We have already seen, in Fig. 3, that the shape of the p_T^γ spectrum is significantly improved by the inclusion of electroweak effects. We therefore extend our prediction for this ratio by taking such corrections into account, rescaling the individual p_T spectra by $(1 + \Delta_{EW}^V)$ as discussed previously. Since the electroweak corrections do not affect the $Z + j$ and $\gamma + j$ processes in the same way [20], this leads to a modification of the prediction for this ratio that is shown in Fig. 8. Although the effects are minor in the low-p_T region, as expected, they become more important in the highest bins. There they decrease the ratio by as much as 7% and thereby improve the agreement with the CMS data.

We now consider a full analysis of the theoretical uncertainties associated with the calculation of $R_{Z/\gamma}^{NNLO+EW}$,

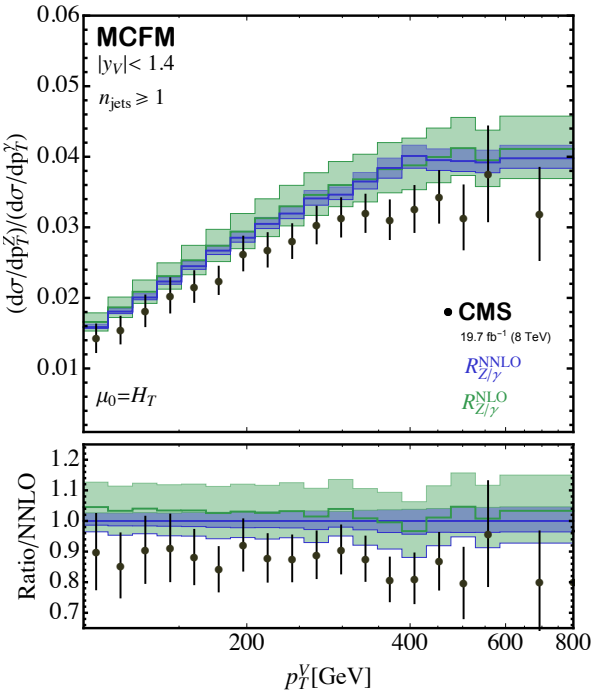

Figure 7: The quantities $R_{Z/\gamma}^{\text{NLO}}(p_T^\gamma)$ and $R_{Z/\gamma}^{\text{NNLO}}(p_T^\gamma)$, defined through Eq. (18), compared to CMS data from ref. [45]. The bands indicate the scale uncertainty on the theoretical predictions.

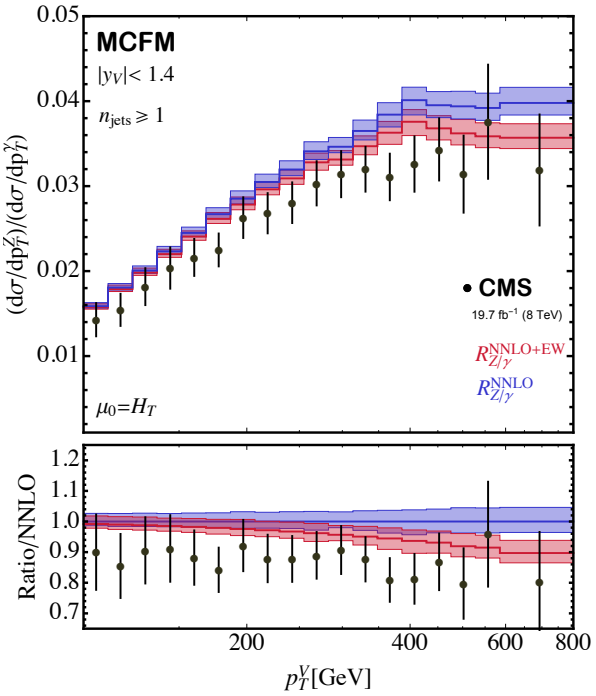

Figure 8: The quantity $R_{Z/\gamma}(p_T^\gamma)$ defined in Eq. (18), computed at NNLO and at NNLO including EW effects, compared to CMS data from ref. [45]. The bands indicate the scale uncertainty on the theoretical predictions.

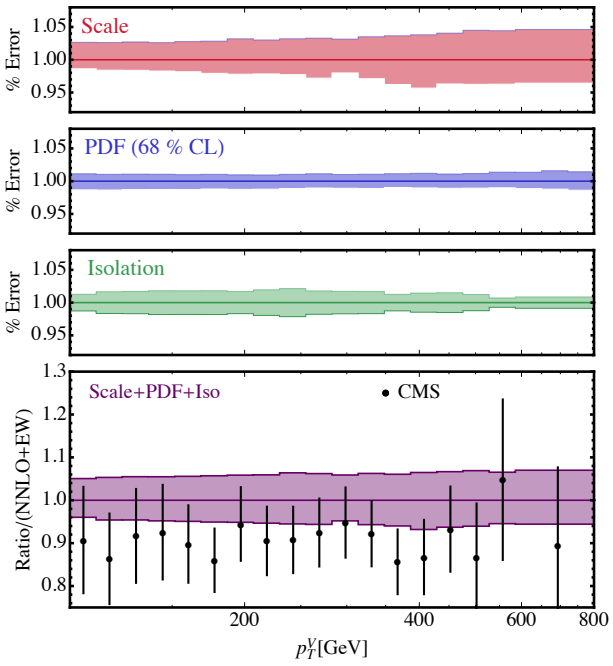

Figure 9: A summary of the theoretical uncertainties discussed in this paper for the Z/γ ratio, $R_{Z/\gamma}^{NNLO+EW}$. In order from the top, uncertainties from: scales, PDFs, isolation and in the total, as described in the main text. The total uncertainty is obtained by combining linearly those from the sources above.

using the same procedure as discussed earlier for the photon p_T spectrum. Our results are presented in Figure 9 where, as before, the uncertainties are normalized to the central value of the combined NNLO QCD + EW prediction. We see that the PDF uncertainties essentially cancel, as one might expect from the nature of the ratio. The dominant uncertainty results from scale variation, especially at high p_T^V. The total uncertainty is only around 4% in the lowest bins and is slightly higher, approximately 6%, at high p_T^V.

As discussed earlier, the asymptotic behavior of our prediction for $R_{Z/\gamma}$ is particularly interesting. In order to quantify this we follow the CMS analysis [45] and define a ratio in which the high-p_T bins are integrated over,

$$R_{\rm dilep} = \frac{\sigma_{\ell^-\ell^+ + j + X}(p_T^V > 314\ {\rm GeV})}{\sigma_{\gamma + j + X}(p_T^V > 314\ {\rm GeV})}\,. \qquad (22)$$

The experimental measurement of this quantity by CMS is,

$$R_{\rm dilep}^{\rm CMS} = 0.0322 \pm 0.0008\ ({\rm stat}) \pm 0.0020\ ({\rm syst})\,.$$

Our best theoretical prediction is provided by the NNLO+EW prediction shown in Figure 8, with accompanying uncertainties illustrated in Figure 9. We find,

$$R_{\rm dilep}^{\rm NNLO+EW}(8\ {\rm TeV}) = 0.0359$$
$$^{+0.0012}_{-0.0013}\ ({\rm scale})\ ^{+0.0004}_{-0.0004}\ ({\rm PDF})\ ^{+0.0006}_{-0.0006}\ ({\rm iso})\,.$$

Given the level of the residual uncertainties, this result is in reasonable agreement with the measured value, $R_{\rm dilep}^{\rm CMS}$.

The CMS collaboration has not yet performed a similar analysis of $\gamma + j$ production at 13 TeV. Since such an undertaking will likely involve a change in the cuts that are applied, or at least in the binning of the final data, for now we refrain from performing a detailed study of individual distributions at this energy. However it is especially important to predict the ratio $R_{Z/\gamma}(p_T)$ and, in particular, its value in the high-p_T tail. For this reason we repeat our above analysis at 13 TeV, with no cuts or input parameters altered apart from the LHC operating energy.

Our prediction for $R_{Z/\gamma}(p_T)$ at 13 TeV is shown in Figure 10, where we compare predictions at NLO, NNLO and when combining NNLO QCD and EW effects. As before (c.f. Figures 7 and 8) we see that the ratio is very similar in all cases, but that the NNLO prediction has a substantially smaller uncertainty and the inclusion of EW effects lowers the ratio at high p_T. At 13 TeV we are further from the large-x region, for the same range of p_T^γ, so that the $\langle u\rangle/\langle d\rangle$ ratio in Eq. (19) is smaller. We thus expect that the value of $R_{\rm dilep}$ is higher at 13 TeV than at 8 TeV, a supposition that is borne out by our explicit calculations. We find, for the asymptotic ratio defined in Eq. (22),

$$R_{\rm dilep}^{\rm NNLO+EW}(13\ {\rm TeV}) = 0.0387$$
$$^{+0.0013}_{-0.0011}\ ({\rm scale})\ ^{+0.0004}_{-0.0004}\ ({\rm PDF})\ ^{+0.0006}_{-0.0006}\ ({\rm iso})\,.$$

We conclude this section with a summary of the theoretical predictions for $R_{\rm dilep}$, computed at various orders of perturbation theory, shown in Figure 11. The improvement in the precision of the theoretical prediction when going from NLO to NNLO QCD is clear. It also emphasizes that, after the inclusion of electroweak effects, there is better agreement between the best theoretical prediction and the measurement of CMS [45]. However some tension still remains in the overall normalization. This could perhaps be relieved somewhat by the use of an alternative electroweak scheme in which the coupling in the $\gamma + j$ process is evaluated at a higher scale rather than using $\alpha(0)$. This would require proper inclusion of the appropriate counterterms in the one-loop EW calculation and such a study is beyond the scope of this work.

V. CONCLUSIONS

In this paper we have presented differential predictions for $\gamma + j$ production at NNLO and compared our predictions to data taken by the CMS experiment at 8 TeV. We have seen that NNLO predictions provide a very good description of the shape of the CMS data, with the inclusion of EW effects improving the agreement further still. For

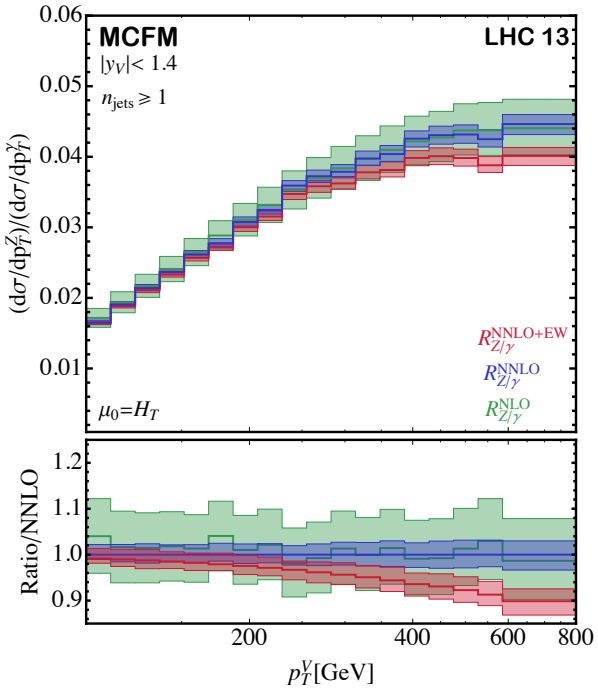

Figure 10: The quantities $R^{\rm NLO}_{Z/\gamma}(p_T^\gamma)$, $R^{\rm NNLO}_{Z/\gamma}(p_T^\gamma)$ and $R^{\rm NNLO+EW}_{Z/\gamma}(p_T^\gamma)$, defined through Eq. (18), for the LHC operating at 13 TeV. The bands indicate the scale uncertainty on the theoretical predictions.

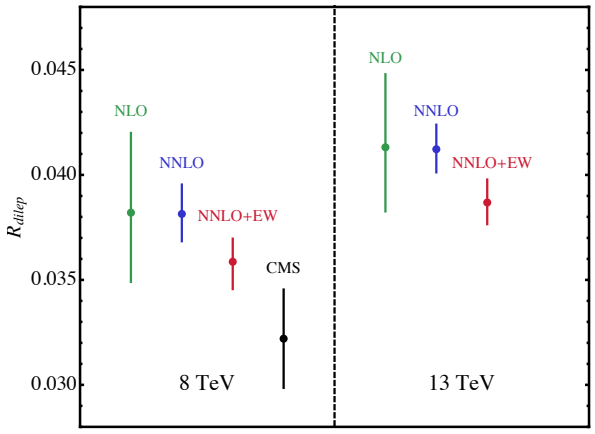

Figure 11: A summary of predictions for, and measurements of, $R_{\rm dilep}$ – defined in Eq. (22) – at 8 and 13 TeV.

the p_T^γ distribution there is an apparent disagreement between the normalization of the theoretical prediction and the observed data, but again the shapes of the theory and data are very similar. We have used our results to compute several other quantities, notably the ratio of $Z+j$ and $\gamma+j$ production as a function of the boson transverse momentum, which is useful for estimating backgrounds to BSM searches. The agreement between the theoretical prediction and data for this ratio is satisfactory. Finally, we have made additional predictions at NNLO accuracy for future studies of the $Z+j/\gamma+j$ ratio at 13 TeV.

p_T^V [GeV]	$R^{\rm NLO}_{Z/\gamma} \times 100$	$R^{\rm NNLO}_{Z/\gamma} \times 100$	$\frac{1+\Delta^Z_{\rm EW}}{1+\Delta^\gamma_{\rm EW}}$
100-111	$1.66^{+0.23}_{-0.21}$	$1.59^{+0.05}_{-0.04}$	0.99
111-123	$1.87^{+0.27}_{-0.24}$	$1.81^{+0.06}_{-0.05}$	0.99
123-137	$2.09^{+0.31}_{-0.28}$	$2.01^{+0.06}_{-0.06}$	0.99
137-152	$2.31^{+0.35}_{-0.32}$	$2.23^{+0.07}_{-0.07}$	0.99
152-168	$2.53^{+0.4}_{-0.36}$	$2.45^{+0.09}_{-0.08}$	0.98
168-187	$2.74^{+0.44}_{-0.39}$	$2.67^{+0.10}_{-0.10}$	0.98
187-207	$2.94^{+0.49}_{-0.43}$	$2.85^{+0.12}_{-0.12}$	0.98
207-230	$3.13^{+0.53}_{-0.47}$	$3.05^{+0.12}_{-0.12}$	0.97
230-255	$3.30^{+0.58}_{-0.5}$	$3.2^{+0.13}_{-0.13}$	0.97
255-283	$3.46^{+0.62}_{-0.54}$	$3.41^{+0.16}_{-0.16}$	0.96
283-314	$3.60^{+0.67}_{-0.57}$	$3.46^{+0.13}_{-0.12}$	0.96
314-348	$3.68^{+0.7}_{-0.6}$	$3.65^{+0.18}_{-0.17}$	0.95
348-386	$3.82^{+0.76}_{-0.64}$	$3.84^{+0.25}_{-0.22}$	0.94
386-429	$3.88^{+0.77}_{-0.65}$	$4.01^{+0.29}_{-0.26}$	0.94
429-476	$4.00^{+0.83}_{-0.69}$	$3.95^{+0.25}_{-0.24}$	0.93
476-528	$4.12^{+0.89}_{-0.73}$	$3.94^{+0.27}_{-0.26}$	0.92
528-586	$3.95^{+0.86}_{-0.71}$	$3.92^{+0.26}_{-0.25}$	0.91
586-800	$4.11^{+0.96}_{-0.78}$	$3.98^{+0.24}_{-0.25}$	0.90

Table I: The values of $R^{\rm NLO}_{Z/\gamma}$ and $R^{\rm NNLO}_{Z/\gamma}$ at 8 TeV (rescaled by a factor of 100), together with the additional correction that corresponds to including EW effects in both processes. Quoted ranges correspond to the variation in the central scale by the six-point method described in the text.

Acknowledgments

We thank Joe Incandela, Jonas Lindert, Michelangelo Mangano and Ruth Van de Water for useful discussions. Support provided by the Center for Computational Research at the University at Buffalo and the Wilson HPC Computing Facility at Fermilab. CW is supported by the National Science Foundation through award number PHY-1619877. The research of JMC is supported by the US DOE under contract DE-AC02-07CH11359.

Appendix

Our numerical results for the $Z+j$ to $\gamma+j$ ratio studied in this paper, $R_{Z/\gamma}$, are presented in Table I (8 TeV) and Table II (13 TeV). For each bin of p_T^V we show the value of the ratio computed to NLO and NNLO accuracy, the associated uncertainty due to scale variation as described in the text, and the EW rescaling factor.

p_T^V [GeV]	$R^{\rm NLO}_{Z/\gamma} \times 100$	$R^{\rm NNLO}_{Z/\gamma} \times 100$	$\frac{1+\Delta^Z_{\rm EW}}{1+\Delta^\gamma_{\rm EW}}$
100.-111.	$1.72^{+0.24}_{-0.22}$	$1.65^{+0.05}_{-0.03}$	0.99
111.-123.	$1.94^{+0.27}_{-0.25}$	$1.91^{+0.05}_{-0.04}$	0.99
123.-137.	$2.17^{+0.3}_{-0.27}$	$2.14^{+0.07}_{-0.06}$	0.99
137.-152.	$2.41^{+0.33}_{-0.3}$	$2.37^{+0.06}_{-0.06}$	0.99
152.-168.	$2.65^{+0.36}_{-0.33}$	$2.61^{+0.07}_{-0.07}$	0.98
168.-187.	$2.88^{+0.40}_{-0.36}$	$2.77^{+0.08}_{-0.08}$	0.98
187.-207.	$3.11^{+0.44}_{-0.40}$	$3.08^{+0.10}_{-0.10}$	0.98
207.-230.	$3.32^{+0.49}_{-0.43}$	$3.25^{+0.11}_{-0.10}$	0.97
230.-255.	$3.53^{+0.54}_{-0.47}$	$3.59^{+0.12}_{-0.11}$	0.97
255.-283.	$3.7^{+0.58}_{-0.51}$	$3.72^{+0.14}_{-0.13}$	0.96
283.-314.	$3.84^{+0.61}_{-0.54}$	$3.79^{+0.15}_{-0.14}$	0.96
314.-348.	$3.97^{+0.65}_{-0.56}$	$3.98^{+0.16}_{-0.15}$	0.95
348.-386.	$4.10^{+0.68}_{-0.59}$	$4.04^{+0.18}_{-0.17}$	0.94
386.-429.	$4.22^{+0.72}_{-0.62}$	$4.26^{+0.18}_{-0.17}$	0.94
429.-476.	$4.27^{+0.75}_{-0.64}$	$4.31^{+0.21}_{-0.19}$	0.93
476.-528.	$4.37^{+0.78}_{-0.66}$	$4.32^{+0.20}_{-0.20}$	0.92
528.-586.	$4.38^{+0.8}_{-0.68}$	$4.25^{+0.19}_{-0.22}$	0.91
586.-800.	$4.40^{+0.84}_{-0.71}$	$4.46^{+0.22}_{-0.24}$	0.90

Table II: The values of $R^{\rm NLO}_{Z/\gamma}$ and $R^{\rm NNLO}_{Z/\gamma}$ at 13 TeV (rescaled by a factor of 100), together with the additional correction that corresponds to including EW effects in both processes. Quoted ranges correspond to the variation in the central scale by the six-point method described in the text.

[1] L. Bergstrom, Annalen Phys. **524**, 479 (2012), 1205.4882.
[2] A. Askew, S. Chauhan, B. Penning, W. Shepherd, and M. Tripathi, Int. J. Mod. Phys. **A29**, 1430041 (2014), 1406.5662.
[3] Z. Bern, G. Diana, L. J. Dixon, F. Febres Cordero, S. Hoche, H. Ita, D. A. Kosower, D. Maitre, and K. J. Ozeren, Phys. Rev. **D84**, 114002 (2011), 1106.1423.
[4] S. Ask, M. A. Parker, T. Sandoval, M. E. Shea, and W. J. Stirling, JHEP **10**, 058 (2011), 1107.2803.
[5] W. T. Giele, E. W. N. Glover, and D. A. Kosower, Nucl. Phys. **B403**, 633 (1993), hep-ph/9302225.
[6] S. Catani, M. Fontannaz, J. Guillet, and E. Pilon, JHEP **0205**, 028 (2002), hep-ph/0204023.
[7] V. Khachatryan et al. (CMS), Phys. Rev. Lett. **106**, 082001 (2011), 1012.0799.
[8] G. Aad et al. (ATLAS Collaboration), Phys.Rev. **D89**, 052004 (2014), 1311.1440.
[9] S. Chatrchyan et al. (CMS Collaboration), JHEP **1406**, 009 (2014), 1311.6141.
[10] G. Aad et al. (ATLAS), JHEP **08**, 005 (2016), 1605.03495.
[11] A. Gehrmann-De Ridder, T. Gehrmann, E. W. N. Glover, A. Huss, and T. A. Morgan, Phys. Rev. Lett. **117**, 022001 (2016), 1507.02850.
[12] R. Boughezal, J. M. Campbell, R. K. Ellis, C. Focke, W. T. Giele, X. Liu, and F. Petriello, Phys. Rev. Lett. **116**, 152001 (2016), 1512.01291.
[13] A. Gehrmann-De Ridder, T. Gehrmann, E. W. N. Glover, A. Huss, and T. A. Morgan, JHEP **07**, 133 (2016), 1605.04295.
[14] R. Boughezal, X. Liu, and F. Petriello, Phys. Rev. **D94**, 074015 (2016), 1602.08140.
[15] J. H. Kuhn, A. Kulesza, S. Pozzorini, and M. Schulze, Phys. Lett. **B609**, 277 (2005), hep-ph/0408308.
[16] J. H. Kuhn, A. Kulesza, S. Pozzorini, and M. Schulze, Nucl. Phys. **B727**, 368 (2005), hep-ph/0507178.
[17] A. Denner, S. Dittmaier, T. Kasprzik, and A. Muck, JHEP **06**, 069 (2011), 1103.0914.
[18] S. Kallweit, J. M. Lindert, P. Maierhofer, S. Pozzorini, and M. Schnherr, JHEP **04**, 021 (2016), 1511.08692.
[19] J. M. Campbell, R. K. Ellis, and C. Williams (2016), 1612.04333.
[20] J. H. Kuhn, A. Kulesza, S. Pozzorini, and M. Schulze, JHEP **03**, 059 (2006), hep-ph/0508253.
[21] J. R. Andersen et al., in *9th Les Houches Workshop on Physics at TeV Colliders (PhysTeV 2015) Les Houches, France, June 1-19, 2015* (2016), 1605.04692, URL http://lss.fnal.gov/archive/2016/conf/fermilab-conf-16-175-ppd-t.pdf.
[22] R. Boughezal, C. Focke, X. Liu, and F. Petriello, Phys. Rev. Lett. **115**, 062002 (2015), 1504.02131.
[23] J. Gaunt, M. Stahlhofen, F. J. Tackmann, and J. R. Walsh, JHEP **09**, 058 (2015), 1505.04794.
[24] J. Gao, C. S. Li, and H. X. Zhu, Phys. Rev. Lett. **110**, 042001 (2013), 1210.2808.
[25] I. W. Stewart, F. J. Tackmann, and W. J. Waalewijn, Phys. Rev. Lett. **105**, 092002 (2010), 1004.2489.
[26] C. W. Bauer, S. Fleming, and M. E. Luke, Phys. Rev. **D63**, 014006 (2000), hep-ph/0005275.
[27] C. W. Bauer, S. Fleming, D. Pirjol, and I. W. Stewart, Phys. Rev. **D63**, 114020 (2001), hep-ph/0011336.
[28] C. W. Bauer and I. W. Stewart, Phys. Lett. **B516**, 134 (2001), hep-ph/0107001.
[29] C. W. Bauer, D. Pirjol, and I. W. Stewart, Phys. Rev. **D65**, 054022 (2002), hep-ph/0109045.
[30] C. W. Bauer, S. Fleming, D. Pirjol, I. Z. Rothstein, and I. W. Stewart, Phys. Rev. **D66**, 014017 (2002), hep-ph/0202088.
[31] J. R. Gaunt, M. Stahlhofen, and F. J. Tackmann, JHEP **04**, 113 (2014), 1401.5478.
[32] J. Gaunt, M. Stahlhofen, and F. J. Tackmann, JHEP **08**, 020 (2014), 1405.1044.
[33] T. Becher and M. Neubert, Phys. Lett. **B637**, 251 (2006), hep-ph/0603140.
[34] T. Becher and G. Bell, Phys. Lett. **B695**, 252 (2011), 1008.1936.
[35] R. Boughezal, X. Liu, and F. Petriello, Phys. Rev. **D91**, 094035 (2015), 1504.02540.
[36] C. Anastasiou, E. W. N. Glover, and M. E. Tejeda-Yeomans, Nucl. Phys. **B629**, 255 (2002), hep-ph/0201274.
[37] T. Gehrmann and L. Tancredi, JHEP **02**, 004 (2012), 1112.1531.
[38] T. Gehrmann, L. Tancredi, and E. Weihs, JHEP **1304**, 101 (2013), 1302.2630.
[39] I. Moult, L. Rothen, I. W. Stewart, F. J. Tackmann, and H. X. Zhu (2016), 1612.00450.
[40] R. Boughezal, X. Liu, and F. Petriello (2016), 1612.02911.
[41] C. Frye, M. Freytsis, J. Scholtz, and M. J. Strassler, JHEP **03**, 171 (2016), 1510.08451.
[42] S. Alioli et al., Submitted to: Working Group Report (2016), 1606.02330.
[43] S. Dulat, T.-J. Hou, J. Gao, M. Guzzi, J. Huston, P. Nadolsky, J. Pumplin, C. Schmidt, D. Stump, and C. P. Yuan, Phys. Rev. **D93**, 033006 (2016), 1506.07443.
[44] A. Buckley, J. Ferrando, S. Lloyd, K. Nordstrom, B. Page, M. Ruefenacht, M. Schoenherr, and G. Watt, Eur. Phys. J. **C75**, 132 (2015), 1412.7420.
[45] V. Khachatryan et al. (CMS), JHEP **10**, 128 (2015), [Erratum: JHEP04,010(2016)], 1505.06520.
[46] S. Frixione and G. Ridolfi, Nucl. Phys. **B507**, 315 (1997), hep-ph/9707345.
[47] J. M. Campbell, R. K. Ellis, Y. Li, and C. Williams, JHEP **07**, 148 (2016), 1603.02663.
[48] M. Cacciari, G. P. Salam, and G. Soyez, JHEP **04**, 063 (2008), 0802.1189.
[49] S. Catani and M. Seymour, Nucl.Phys. **B485**, 291 (1997), hep-ph/9605323.
[50] T. Becher and X. Garcia i Tormo, Phys. Rev. **D88**, 013009 (2013), 1305.4202.
[51] T. Becher and X. Garcia i Tormo, Phys. Rev. **D92**, 073011 (2015), 1509.01961.
[52] A. Gehrmann-De Ridder and E. N. Glover, Nucl.Phys. **B517**, 269 (1998), hep-ph/9707224.
[53] S. Catani, M. Fontannaz, J. P. Guillet, and E. Pilon, JHEP **1309**, 007 (2013), 1306.6498.
[54] D. d'Enterria and J. Rojo, Nucl. Phys. **B860**, 311 (2012), 1202.1762.
[55] L. Carminati, G. Costa, D. D'Enterria, I. Koletsou, G. Marchiori, J. Rojo, M. Stockton, and F. Tartarelli, Europhys. Lett. **101**, 61002 (2013), 1212.5511.